MESOSPHERIC MOTIONS OVER BEAR LAKE

C.S. Fish, F.T. Berkey
Space Dynamics Laboratory – Utah State University

Abstract

Since February 1999, the Utah State University Bear Lake Observatory (41.9°N, 111.4°W) dynasonde has been configured to operate as an Imaging Doppler Interferometer (IDI). Imaging Doppler interferometry is one of a number of MF/HF radar techniques used to estimate mesospheric winds and dynamics. This paper presents results of the mesospheric (50 – 115 km) background wind, tides, and planetary waves as derived from analysis of IDI observations recorded between February 03, 1999 and February 21, 2000 at Bear Lake.

Imaging Doppler Interferometry

The term imaging Doppler interferometry was first coined by Adams and coworkers [*Adams et al.*, 1985; *Adams et al.*, 1986] to describe a pulsed-radar technique they developed for acquiring 3D "images" of middle atmospheric MF/HF partial reflections. There are a number of possible explanations for the physical origin of the MF/HF partial reflections. A most plausible explanation seems to be of scattering from irregularities in electron density due to atmospheric turbulence [*Roper*, 1998]. The partial reflection "echoes" appear to be discrete in nature and to move with the local bulk motion of the neutral wind. As such, the echoes are useful as tracers of the neutral wind.

Imaging Doppler interferometry uses a combination of Doppler sorting and spatial interferometry to describe the motion and location of the MF/HF echoes. Assuming that the echoes within the illuminated radar zone move with identical horizontal velocities, each echo is then uniquely identifiable by its radial velocity using simple Doppler analysis. The Doppler phase spectrum allows for the use of radar interferometric techniques [*Farley et al.*, 1981; *Kudeki et al.*, 1981; and *Providakes et al.*, 1981] to locate the echoes in 3D space. A 3D vector fit of the echoes characterizes neutral wind motion.

Implementation of the dyansonde as an IDI

The dynasonde [*Wright*, 1969] is a National Oceanic and Atmospheric Administration HF radar [*Grubb*, 1979]. It is a general-purpose pulse-amplitude computer-based radar system for radio measurements of the ionosphere. It has a frequency transmission range of 0.1 to 30 MHz. Having a dual-channel receiver, it supplies fast measurements of such wave components as polarization, amplitude, phase, and direction of arrival [*Davies*, 1990].

The Bear Lake dynasonde has typically been operated as an ionosonde. As an ionosonde, swept frequency soundings are made periodically (every 5 minutes) to map the bottomside of the ionosphere. Transmission is made on a 1.5 MHz resonant horizontal traveling-wave dipole with a peak output of 10 kW. The receiving antenna array lies 150 meters north of the transmitting antenna and is comprised of four 11 MHz resonant horizontal dipoles in an L-shaped pattern termed the L-werpol [after *Jarvis and Dudeney*, 1986] as shown in Figure 1. The dual-channel dynasonde receivers are multiplexed to allow sampling of any variation of the N-S and E-W receiving arrays.

The computer-based control of the dynasonde proves for easy implementation of the dynasonde as an IDI. The imaging Doppler interferometry technique was first adapted to the dynasonde by colleagues at the British Antarctic Survey (BAS) using the Halley (76°S, 26°W) dynasonde [*Jones et al.*, 1997]. Only software modifications were necessary to implement the Halley dynasonde as an IDI. Recently [*Charles and Jones*, 1999], a complete year of results form the Halley IDI data was published. The findings were very similar to other southern high latitude sites and further established the imaging Doppler interferometry technique as a viable tool for long term observations of the middle atmospheric neutral wind.

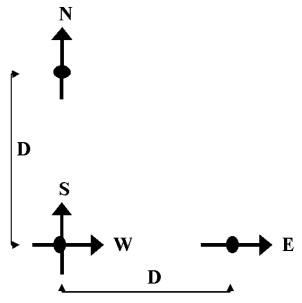

Figure 1. The physical configuration of the L-werpol receiving antenna array

The operating system of the Bear Lake dynasonde is essentially identical to that at Halley. BAS made their software modifications available to us in 1998. The Bear Lake dynasonde was subsequently configured to operate as a full-time IDI in February of 1999. In IDI mode, the Bear Lake dynasonde transmits at 2.2 MHz during the evening and early morning hours (00-13 hr UT) and 3.8 MHz during the daytime (13-24 hr UT) to reduce D-region absorption effects. Transmissions are made periodically (at 5 minute intervals), interspersed with regular ionosonde soundings. A four-pulse set of 48 μs square pulses is transmitted every 0.8 s with a total of 1024 such pulse sets in each IDI sounding. The inter-pulse period of the individual pulse-set pulses is 0.01 s with an N-S or E-W antenna pair (see Figure 1) sampling occurring for each pulse. Antenna spacing ($D \approx 30$ meters, see Figure 1) ensures that IDI echoes can be received from zenith angles greater than ~70°before phase aliasing occurs. A height range of 50 - 115 km is scanned with ADC sampling rates limiting height resolution to ± 0.75 km. Echo returns are sorted into 5 km height bins with all subsequent data analysis performed at 5 km height intervals. See section 3 of *Jones et al.* [1997] for a comprehensive description of the imaging Doppler interferometry technique data analysis as implemented on the Halley and Bear Lake dynasondes.

Observations

The IDI system parameters optimize the dataset against statistical uncertainty in the wind measurements and provide a sufficiently high-resolution dataset to allow monitoring of the wind variations with height and time [*Charles and Jones*, 1999]. The temporal resolution is insufficient to provide information on gravity waves (periods of 30 min. or less) but lends itself very well to the study of longer period tides and planetary waves. The following sections present the results of analysis of a complete year of Bear Lake IDI data between February 03, 1999 and February 21, 2000. The only significant radar down time occurred between February 11 – 17, 1999. In all figures, the height bins are in 5 km intervals (*i.e.*, 70 km represents 70 – 75 km and 110 km represents 110 – 115 km).

Number of Echoes

A majority of the MF/HF echoes occur between 70 and 115 km, however echoes are often recorded to as low as 50 km. The higher altitudes have greater levels of electron density and turbulence [*Hocking*, 1988] resulting in greater electron density gradients. This further supports the hypothesis that turbulence is a principle factor in the creation of the MF/HF partial reflection scattering points [*Roper*, 1998]. As seen in Figure 2, the average number of echoes per sounding per day are at maxima in the summer and winter months. Minima occur during the equinoxes, but even at these times the number of echoes is sufficient to allow continuous wind measurements. The minima occur when the mean winds (see Figure 3) are changing direction. A similar pattern was seen at Halley [*Charles and Jones*, 1999]. A notable difference between Halley and Bear Lake echo counts is that the number of average echoes per sounding per day is roughly a factor of 3 greater in the Bear Lake IDI data.

Mean Winds

Figure 3 shows the mesospheric mean wind variations for the meridional (top panel) and zonal components. A ten-day running mean was calculated every 3 days on 5 minute wind sequences to reduce the effects of tidal oscillations. The direction and strength (amplitude) of the components is indicated by the filled contours.

Meridional

Meridional mean winds are predominantly equatorward in the summer at all heights with maximum velocities of 15 m/s. In the spring and early fall, there is no dominant pattern and the winds appear rather stationary. The winter winds are generally poleward with maximum velocities of ~10 m/s. Throughout the year there appears to be a slight bias for equatorward winds. Of note is the "beating" effect most observable during the summer months with a period of 10 – 20 days.

Zonal

Zonal mean winds are westward at all heights during the late spring and early summer. Maximum velocities of 25 m/s are reached. The wind field changes radically in the late summer to that of eastward motion with maximum velocities of ~ 20 m/s between 100 and 115 km. The winter months have a strong westward flow (25 m/s maximum) below 95 km with an inconsistent eastward flow (20 m/s maximum) at greater altitudes. The periodic 10-20 day beating seen in the meridional winds is even more evident in the zonal winds.

Tides and Planetary Waves

The dataset was analyzed for periodic tidal and planetary wave oscillations. Figures 4 through 6 are yearlong spectrograms of the 95-100 km height range as it was felt that this height was fairly representative of

the patterns seen in the mean winds. The spectrograms were calculated on 1-hour mean wind sequences by sliding a 43 day long periodogram at 5-day intervals. The computations used a fast Fourier transform algorithm with a Tukey filter to smooth the edges of the sampling window in order to reduce sidelobe contamination [*Jones et al.*, 1997]. The top panel shows the frequency content of the meridional component and the bottom panel is of the zonal component. Figure 4 emphasizes the tidal components (*i.e.*, higher frequency (shorter period) per day components) of the 95 – 100 km winds. Figures 5 and 6 more clearly show the longer period waves (*e.g.*, 2-day, 6-day, 16-day planetary waves).

Figures 7 and 9 show the amplitudes of sinusoidal fits of 24, 12, and 8 hr (*i.e.*, diurnal, semidiurnal, and terdiurnal, respectively) tides for all heights throughout the year-long dataset. Least squares fits were made on ½ hour mean wind sequences over a 10-day window that was incremented every 2 days. The fits were made for a constant wind (A_O), a 2-day planetary wave (A_{48}) and phase (P_{48}) and 24, 12, and 8 hr tidal amplitudes (A_{24}, A_{12}, A_8) and phases (P_{24}, P_{12}, P_8) according to the equations:

$$f = A_O + A_{48} \cdot \sin\left(\frac{2\pi}{48}t - P_{48}\right) + A_{24} \cdot \sin\left(\frac{2\pi}{24}t - P_{24}\right) + A_{12} \cdot \sin\left(\frac{2\pi}{12}t - P_{12}\right) + A_8 \cdot \sin\left(\frac{2\pi}{8}t - P_8\right)$$

Figure 7 is of the meridional component and Figure 9 is of the zonal component. Figures 8 and 10 show the amplitudes for sinusoidal fits of 16-day, 6-day, 3-day, and 2-day planetary waves tides for all heights throughout the year-long dataset. Least squares fits were made on ½ hour mean wind sequences over a 20-day window that was incremented every 2 days. The fits were made for a constant wind (A_O) and 16, 6, and 3-day wave amplitudes (A_{16d}, A_{6d}, A_{3d}) and phases (P_{16d}, P_{6d}, P_{3d}) according to the equations:

$$f = A_O + A_{16d} \cdot \sin\left(\frac{2\pi}{16d}t - P_{16d}\right) + A_{6d} \cdot \sin\left(\frac{2\pi}{6d}t - P_{6d}\right) + A_{3d} \cdot \sin\left(\frac{2\pi}{3d}t - P_{3d}\right)$$

Figure 8 is of the meridional component and Figure 10 is of the zonal component. In Figures 4 through 10, note that the background plot color is white. This can initially be misleading as the maximum contour values are also referenced to white.

Diurnal and Semidiurnal Tides

Meridional

As seen in Figures 4 and 7, the meridional diurnal tide reaches peak values (~ 17 m/s) during the winter, spring, and early summer. It is virtually non-existent in the late summer and early fall. It is strongest in late winter and early spring between 75 and 115 km. The meridional semidiurnal tide dominates the diurnal tide above 90 km throughout most of the year. In general, the semidiurnal tide magnitude is a factor of 2 greater (~ + 35 m/s) than the diurnal tide. This is expected as the vertical wavelength of the semidiurnal tide is much larger than the diurnal tide at these heights and latitude [*Smith*, 2000; *Hargreaves*, 1995]. The most dominant period of the semidiurnal tide occurs in conjunction with the strong summer equatorward meridional mean winds of Figure 3. The semidiurnal tide is present down to heights of 80 km at this time.

Zonal

The zonal diurnal tide is only evident in the late winter through the early summer months in Figures 4 and 9. However, it reaches magnitudes of ~ 28 m/s as compared to 17 m/s in the meridional component. It is non-existent from late summer to mid-winter. The zonal semidiurnal tide is not as dominating as the meridional component. It is mainly present from late spring to late summer. The zonal semidiurnal tide magnitude is very similar to the meridional component during these months (peaks of ~ 35 m/s). Once again, the most dominant period of the semidiurnal tide occurs in conjunction with a dominant period of mean wind motion. In Figure 3, the zonal winds are strongly westward from late spring to mid-summer.

Terdiurnal Tides

Meridional

In Figures 4 and 7, the meridional terdiurnal tide is much weaker than the diurnal and semidiurnal tides throughout the year. It is most evident in the late fall. It reaches a peak of ~ 8 m/s and is seen between 80 and 115 km.

Zonal

In Figures 4 and 9, the zonal terdiurnal tide is stronger than the meridional terdiurnal tide but is still much weaker than the zonal diurnal and semidiurnal tides. It reaches a peak of ~ 8 m/s and is most observable in the fall.

The terdiurnal tide results are in good agreement with other northern mid-latitude observations [*Smith*, 2000; *Pendleton et al.*, 2000; *Taylor et al.*, 1999] where the terdiurnal tide was most evident in the fall with a magnitudes of 5 – 15 m/s.

Planetary Waves

Meridional

Figures 5 and 8 clearly show a meridional 2-day planetary wave wind component. It is particularly enhanced in the summer and reaches a peak magnitude of ~ 15 m/s It occurs between 70 and 115 km. These characteristics are very typical of other northern latitude 2-day wave results [*Meek et al.*, 1996; *Clark et al.*, 1994]. Figures 6 and 8 show strong evidence of meridional 6 and 16-day planetary wave wind component. In Figure 6, dotted lines corresponding to the wave periods are given in ascending order (*i.e.*, least to greatest period) for better visual identification of the waves. Both the 6 and 16-day waves occur predominantly in the fall and winter months between 80 and 115 km. They also both reach peaks of ~ 13 m/s. Furthermore, there is also evidence of meridional 3.8 and 5-day waves in Figure 6.

Zonal

Figures 5 and 10 show a weak zonal 2-day planetary wave wind components. Similar to the meridional 2-day wave, it is present in the summer and reaches a peak of ~ 15 m/s It occurs between 85 and 115 km. Figures 6 and 10 show strong evidence of zonal 3 and 16-day planetary wave wind components. The 3-day wave occurs predominantly in the fall and winter between 80 and 115 km. It reaches a peak of ~ 8 m/s. The 16-day wave is present in both the summer and winter. From Figure 6, there is also evidence of 6, 8.3, 10, and 20-day waves.

The meridional and zonal planetary wave results are very similar to the findings of other researchers [*Luo et al.*, 2000; *Manson and Meek*, 1986; *Jacobi et al.*, 1998]. Manson and Meek found that at northern mid-latitudes (Saskatoon (52°N, 107°W)) 2-day waves maximize in the summer while longer period waves tend to maximize in the winter.

Conclusion

In this paper we have presented results from the first complete year (February 03, 1999 – February 21, 2000) of IDI observations at Bear Lake. The technique has provided very reliable measurements of the mean wind, tidal oscillation, and long-period planetary wave motion in the middle atmosphere (60 – 115 km). The mean meridional winds blow southward in the summer followed by a mixture of southward and northward winds throughout the rest of the year. The mean zonal winds are stronger (~ factor of two) and have more highly defined regions of transition than the meridional winds. They are mainly westward in the late spring and early summer, eastward in the late summer and early fall, eastward above 85 km in the winter, and westward below 85 km in the winter. The meridional and zonal semidiurnal tide dominates the diurnal tide throughout the year. It is most evident in the summer with amplitudes near 40 m/s. The diurnal tide is most observable in the winter. Both the semi- and diurnal tidal components increase in magnitude with height. The terdiurnal (8 hr) tide is weakly present throughout the year and strongest in the fall (magnitudes of ~ 10 m/s). The 2-day planetary wave is clearly seen in the summer. Other planetary waves (*e.g.*, 3, 6, 16, and 20 day period waves) are very evident in the fall and winter.

The IDI at Bear Lake continues to accumulate data and will be a very useful technique for future short- and long-term study of the middle atmosphere.

Acknowledgements

The authors would like to thank our colleagues at BAS, in particular Owen Jones, for their past and continued support in implementing the Bear Lake dynasonde as an IDI. The authors would also like to recognize the support of Space Dynamics Laboratory – Utah State University. This material is based upon work supported by the Rocky Mountain Space Grant Consortium and the National Science Foundation under grant OPP95-30935.

References

Adams, G.W., D.P. Edwards, and J.W. Brosnahan, The imaging Doppler interferometer: Data analysis, *Radio Sci.*, **20**, 1481-1492, 1985.

Adams, G.W., J.W. Brosnahan, D.C. Walden, and S.F. Nerney, Mesospheric observations using a 2.66-MHz radar as an imaging Doppler interferometer: Description and first results, *J. Geophys. Res.*, **91**, 1671-1683, 1986.

Charles, K., G.O.L. Jones, Mesospheric mean winds and tides observed by the imaging Doppler Interferometer (IDI) at Halley, Antarctica, *J. Atmos. Solar-Terr. Phys.*, **61**, 351-362, 1999.

Clark, R.R., A.C. Current, A.H. Manson, C.E. Meek, S.K. Avery, S.E. Palo, and T. Aso, Hemispheric properties of the two-day wave

from mesopshere-lower-thermosphere radar observations, *J. Atmos. Sol-Terr. Phys.*, **56**, 1279-1288, 1994.

Davies, K., ***Ionospheric Radio***, Peter Peregrinus Ltd., London, 1990.

Farley, D.T., H.M. Ierkic, and B.G. Fejer, Radar interferometry: A new technique for studying plasma turbulence in the ionosphere, *J. Geophys. Res.*, **86**, 1467-1472, 1981.

Grub, R.N., The NOAA SEL HF radar system (ionospheric sounder), *Tech. Memo. ERL-SEL 55*, Natl. Oceanic and Atmos. Admin., Boulder, Colo., 1979.

Hargreaves, J.K., ***The solar-terrestrial environment***, Cambridge University Press, Cambridge, 1995.

Hocking, W.K., Two years of continuous measurements of turbulence parameters in the upper mesosphere and lower thermosphere made with a 2-MHz radar, *J. Geophys. Res.*, **93**, 2475-2491, 1988.

Jacobi, C., R. Schminder, and D. Kürschner, Planetary wave activity obtained form long-period (2-18 days) variations of mesopause region winds over central Europe (52°N, 15°E), *J. Atmos. Sol-Terr. Phys.*, **60**, 81-93, 1998.

Jarvis, M.J., and J.R. Dudeney, *Radio Sci.*, **21**, 151-158, 1986.

Jones, G.O.L. K. Charles, and M.J. Jarvis, First mesospheric observations using an imaging Doppler interferometer adaptation of the dynasonde at Halley, Antarctica, *Radio Sci.*, **32**, 2109-2122, 1997.

Kudeki, E., B.G. Fejer, D.T. Farley, and H.M. Ierkic, Interferometer studies of equatorial F region irregularities and drifts, *Geophys. Res. Lett.*, **8**, 377-380, 1981.

Luo, Y., A.H. Manson, C.E. Meek, C.K. Meyer, and J.M. Forbes, The quasi 16-day oscillations in the mesosphere and lower thermosphere at Saskatoon (52°N, 107°W), 1980-1996, *J. Geophys. Res.*, **105**, 2125-2138, 2000.

Manson, A.H., and C.E. Meek, Dynamics of the middle atmosphere at Saskatoon (52°N, 107°W): A spectral study during 1981, 1982, *J. Atmos. Terr. Phys.*, **48**, 1039-1055, 1986.

Meek, C.E., A.H. Manson, S.J. Franke, W. Singer, P. Hoffmann, R.R. Clark, T. Tsuda, T. Nakamura, M. Tsutsumi, M. Hagan, D.C. Fitts, J. Isler, and Yu I. Protnyagin, Global study of northern hemisphere quasi-2-day wave events in recent summers near 90 km altitude, *J. Atmos. Terr. Phys.*, **58**, 1401-1411, 1996.

Pendleton, W.R., Jr., M.J. Taylor, and L.C. Gardner, Terdiurnal oscillations in OH Meinel rotational temperatures for fall conditions at norther mid-latitude sites, *Geophys. Res. Lett.,* accepted April 2000.

Providakes, J.F., W.E. Swartz, D.T. Farley, and B.G. Fejer, First VHF auroral radar interferometer observations, *Geophys. Res. Lett.*, **10**, 401-404, 1983.

Roper, R.G., On the reality of upper mesospheric/lower thermospheric turbulent “eddies”, *Radio Sci*., 33, 67-82, 1998.

Smithe, A.K., Structure of the terdiurnal tide at 95 km, *Geophys. Res. Lett.*, 27, 177-180, 2000.

Taylor, M.J., W.R. Pendleton, Jr., C.S. Gardner, and R.J. States, Comparison of terdiurnal tidal oscillations in mesospheric OH rotational temperature and Na lidar temperature measurements at mid-latitudes for fall/spring conditions, *Earth Planets Space*, **51**, 877-885, 1999.

Wright, J.W., *Proc. IEEE.*, **57**. 815-825, 1969.